Plasma Sources Sci. Technol. 4 (1995) 317–331. Printed in the UK

A two-region model of a radiofrequency low-pressure, high-density plasma

Richard S Wise, Dimitris P Lymberopoulos and Demetre J Economou

Plasma Processing Laboratory, Department of Chemical Engineering, University of Houston, Houston, TX 77 204-4792, USA

Received 11 July 1994, in final form 21 November 1994

Abstract. A two-region model of a low-pressure, high-density RF excited discharge was developed. A well-mixed bulk plasma model was coupled to a collisionless sheath to predict the species density, the time-dependent electron-velocity distribution function and the ion bombardment flux and energy. The model was applied to a chlorine discharge sustained in a transformer-coupled plasma reactor. The discharge was found to be moderately electronegative; the negative ion to electron density ratio increased with increasing pressure, decreasing power and/or increasing wall recombination probability γ of the Cl atoms. Under these conditions the dominant ion was Cl_2^+. On the other hand, low pressure, high power and/or small γ resulted in a large degree of gas dissociation; the dominant ion was then Cl^+. The ion flux to the walls increased linearly with power and decreased with pressure. The model predictions were in reasonable quantitative agreement with experimental measurements. The model is most useful for sorting out the complex chemistry of plasmas and for rapid evaluation of expected reactor performance.

Nomenclature

E	electric field (V cm^{-1})
h_L, h_R	shape factors for ion flux, equations (11) and (12)
I_j	current density due to species j (A cm^2)
I_{sj}	sheath current density due to species j (A cm^2)
k	Boltzmann's constant (eV K^{-1})
k_{att}	attachment rate coefficient (cm^3 s^{-1})
k_d	dissociation rate coefficient (cm^3 s^{-1})
k_{ei}	Cl_2^+-electron dissociative recombination rate coefficient (cm^3 s^{-1})
k_{i1}	atomic Cl ionization rate coefficient (cm^3 s^{-1})
k_{i2}	molecular Cl_2 ionization rate coefficient (cm^3 s^{-1})
$k_j(\phi)$	time-dependent electron impact rate coefficient for process j (cm^3 s^{-1})
k_{ij}	ionization rate coefficient of particle j (cm^3 s^{-1})
k_{ii}	ion–ion recombination rate coefficient (cm^3 s^{-1})
$k_{sr,j}$	recombination rate coefficient on surface j (cm s^{-1})
k_{vr}	rate coefficient for volume recombination of Cl (cm^6 s^{-1})
L	reactor (bulk plasma) height (cm)
m	electron mass (g)
M_i	mass of species i (g)
n_i	number density of species i (cm^{-3})
n_e	electron density (cm^{-3})
N	total gas density (cm^{-3})
P	power
r_s	rate of surface reaction (cm^{-2} s^{-1})
R	reactor radius (cm)
R_s	substrate radius (cm)
S_j	area of surface j (cm^2)
t	time (s)
T_e	electron temperature (K)
T_g	gas temperature (K)
u_{Bi}	Bohm velocity for Cl^+ ($i = 1$) or Cl_2^+ ($i = 2$)
v_{th}	thermal velocity (cm s^{-1})
V_{DC}	DC potential of the substrate (V)
V_f	floating potential (V)
V_p	plasma potential (V)
V_{RF}	RF potential of substrate (V)
V_w	wall potential (V)
γ	surface reaction probability of Cl atoms
ε	electron energy (eV)
$\langle\varepsilon\rangle$	mean electron energy (eV)
ε_+	energy of ions striking wall (eV)
ε_0	permittivity of free space (F cm^{-1})
λ_j	mean free path of species j (cm)
$\sigma_j(\varepsilon)$	electron collision cross section for process j (cm^2)
τ_{res}	gas residence time (s)
ϕ	phase angle
ω	excitation frequency (rad s^{-1})

0963-0252/95/030317+15$19.50

1. Introduction

Plasma etching and deposition of thin films are crucial operations in the manufacturing of microelectronic circuits. As device dimensions continue to shrink, process requirements become ever more stringent. For example, fabrication of the next generation devices requires accurate patterning of linewidths less than 0.35 μm, uniformity better than a few percent over wafers of > 200 mm diameter and no radiation damage. In order to meet these demands, new plasma sources, termed high-density plasmas (HDPs), are currently under active development [1]. These sources operate at low gas pressure (0.1–50 mTorr) to help achieve better etching anisotropy and uniformity (low pressure may also result in less contamination), and high plasma density (> 10^{11} cm^{-3}) to enhance etching rate. Examples include inductively (or transformer) coupled plasmas (ICP or TCP), helicon, helical resonator and electron cyclotron resonance (ECR) plasmas [1].

Mathematical models and numerical simulations can provide valuable insight into plasma reactor performance as design and operating conditions vary, and can aid in the development of new plasma sources. Although large-scale global reactor simulations provide a wealth of information on the spatiotemporal plasma dynamics [2, 3], these simulations are computationally expensive. An alternative approach separates the reactor into two regions, namely bulk plasma and sheath (see figure 1). A model is written for each region, and the two models are 'patched' at the plasma–sheath interface. This approach was developed for capacitively coupled reactors [4, 5], but it can be extended to HDP sources [6]. The two-region model can be very useful for sorting out the complex chemistry of mixed-gas plasmas. Importantly, the short CPU time requirements of the two-region model allow detailed evaluations of the plasma chemistry through sensitivity analysis. The dominant chemical reactions thus identified can then be used in a large-scale simulation to obtain a complete picture of the spatiotemporal plasma dynamics.

In this paper we present a two-region model of a radiofrequency low-pressure, high-density plasma source. A chlorine discharge sustained in a TCP/ICP source is considered as a case study. However, the model can be applied to other gases, including mixed-gas plasmas, as well as other HDP sources. For example, we have applied the same model to a chlorine–argon mixture. Our goal here is to demonstrate the approach rather than present applications to many different systems.

Previous work on the subject related to HDP sources has been reported by Lieberman and Gottscho [1] for an argon discharge and recently by Lee *et al* [6] for an oxygen discharge. Lee *et al* [6], assumed a Maxwellian electron-energy distribution function (EEDF) and solved for a steady-state discharge (no time-dependent electron density and electron-impact rate coefficients). In our approach, we solve for the EEDF, and we also consider the time-dependence of the electron properties (density and energy) and the electron-impact reaction rate coefficients.

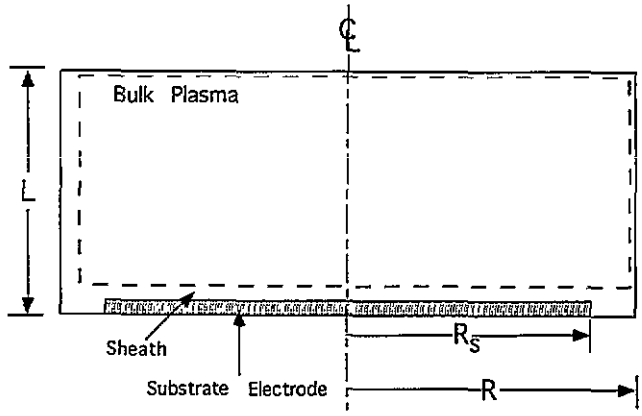

Figure 1. A schematic diagram of a cylindrical high-density plasma source. The reactor is separated into bulk plasma and sheath. The substrate may be biased. The sheath thickness is shown exaggerated for clarity.

2. The development of the model

A schematic diagram of the reactor is shown in figure 1. The plasma is generated by RF coils. The substrate electrode may or may not be biased by a separate RF source. The main assumptions of the model are the following.

(i) The bulk plasma is 'well mixed'. This assumption implies that all species densities and electric field are spatially uniform in the bulk plasma. Despite the low operating pressures, species gradients may still exist, especially for electrons and ions. However, we use this assumption for simplicity. A correction factor based on work by Godyak [7] is used to account for the drop in the positive ion density from the bulk plasma to the sheath edge. Alternatively, an ambipolar diffusion profile could be used for the charged species.

(ii) The sheath is collisionless. This is an excellent assumption for the range of operating conditions considered in this work. The sheath is only a few Debye lengths λ_D (λ_D < 100 μm) thick, while the charged species mean free path is about 1 cm at 10 mTorr. The fact that the sheath is collisionless is highly advantageous from the computational point of view. The actual potential distribution in the sheath is not needed in order to determine the energy of charged particles striking the wall. One needs to know only the *potential difference* between the plasma and the wall. Also, the ion flux striking the wall is equal to the ion flux entering at the sheath edge. Finally, the exact location of the bulk plasma–sheath interface is immaterial in determining the charged particle flux and energy, as long as the correct potential difference is used.

(iii) Because the sheaths are so thin, the dimensions of the bulk plasma are essentially those of the vessel.

(iv) The bulk plasma is electrically neutral. This assumption is approximately correct since significant charge separation occurs over a length scale equal to λ_D while the dimensions of the bulk plasma are of order several centimetres.

(v) The total number density of species in the reactor is constant.

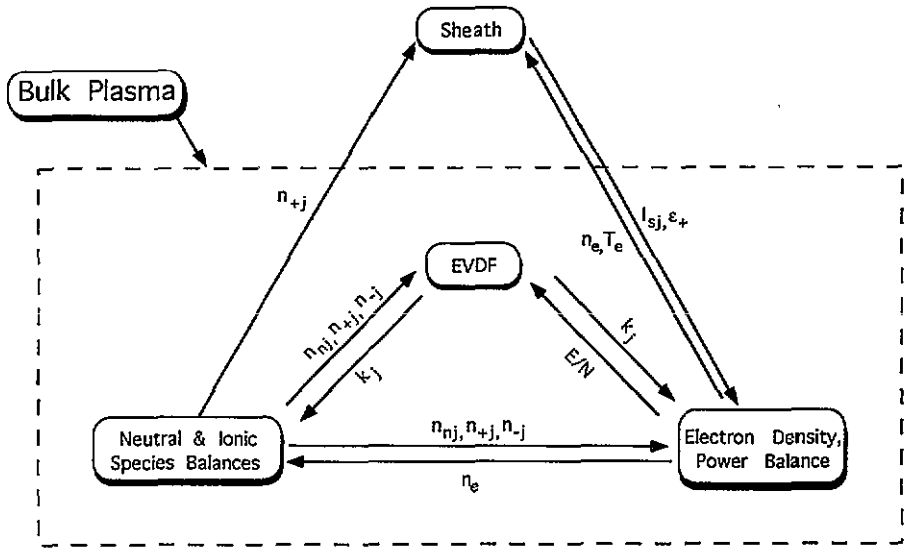

Figure 2. An overview of the modular approach used to speed up calculations. Information exchange between the modules is shown. Subscript e refers to electrons. Subscripts n, + and − refer to neutrals, positive ions and negative ions respectively.

(vi) A neutral energy balance is not included at the present stage of the model. The gas temperature was assumed constant at $T_g = 500$ K, as determined for the bulk plasma under similar conditions by direct simulation Monte Carlo methods.

The goal is to determine the density of the charged and neutral species, the self-sustaining electric field and the electron velocity distribution function (EVDF) in the bulk, and the energy and flux of ions striking the walls for given system geometry and operating parameters (gas flow, pressure, frequency, power, wall material and potential, and so on). In order to achieve this goal, a coupled system of equations is solved, including conservation equations for species density, a power balance, the Boltzmann equation for the EVDF and sheath equations. In order to improve the computational efficiency further, the system is decomposed into four modules, coupled with one another as shown in figure 2.

(i) Module I, the dynamic Monte Carlo (DMC) simulation module, determines the EVDF for given electric field and plasma composition (neutral and charged species densities). Cross sections for all reactions involving electrons are also required as input to this module. From the EVDF, electron-impact reaction rate coefficients are calculated for use in the other modules.

(ii) Module II consists of electron density and power balance equations to determine the self-sustaining electric field and electron density. It requires the neutral and ionic species densities, power delivered to the system and reaction rate coefficients as input.

(iii) Module III consists of mass balance equations for the neutral and ionic species, and provides the density of these species. It requires the electron density and reaction rate coefficients as input.

(iv) Module IV, the sheath module, uses an analytic expression for the collisionless sheath over a substrate, which can be floating, earthed or biased. It provides the flux and energy of charged particles striking the wall. It requires knowledge of the charged species density and electron energy at the sheath edge, as well as information about the electrical state of the wall (floating, earthed or biased).

The modular approach is convenient since one can take advantage of the physics of the problem to speed up the calculation. For example, neutral and ionic species are too massive to respond to the changes in the RF (13.56 MHz) field. Furthermore, neutral and ionic species reactions can occur on time scales of tens of milliseconds. Hence, the density of these species attains an essentially time-independent 'quasi-steady' state. In contrast, electrons respond on a nanosecond time scale and hence can follow the variations in the field. Hence the electron-impact reaction rate coefficients (module I) and electron density (module II) can be modulated at 13.56 MHz. By artificially splitting the equations describing processes with vastly different time scales (nanoseconds versus milliseconds) one avoids the tedious time integration over many hundreds of thousands of RF cycles, which would otherwise be needed in order to achieve the periodic steady-state condition of the self-sustained discharge.

The flow of information is also shown in figure 2. Information is cycled back and forth among the modules until convergence is attained. In the two-region formulation, modules I, II and III constitute the bulk plasma, while module IV is the sheath. A detailed description of each module is given below.

2.1. The bulk plasma

2.1.1. Module I: dynamic Monte Carlo simulation. This module uses a stochastic simulation referred to as

the dynamic Monte Carlo simulation [8] to solve for the EVDF and in turn to provide the rate coefficients of electron-impact reactions. These coefficients are in general phase-shifted with respect to the sinusoidal sustaining electric field because, at low pressures, the energy relaxation frequency is lower than the applied frequency of 13.56 MHz. Hence the quasi-steady-state approximation, which is valid at pressures exceeding several hundred milli-Torr [9, 10], cannot be used under the present conditions.

Module I requires cross section data of electron collisions, the electric field and the plasma composition as input. These quantities are known at the beginning of any given instance of the DMC module being called upon. The trajectory of an electron in free flight is described by integrating Newton's equations of motion. The probability that the electron will not experience a collision is given by

$$P^{NC} = 1 - \sum_{i,j} P_{ij}^{C}$$
$$= 1 - \Delta t \sum_{i,j} n_j u_0 2\pi \int_0^{\pi} \sigma_{ij}(u_0, \chi') \sin\chi' \, d\chi' \qquad (1)$$

whereas the probability that the electron will suffer a collision of type i with a particle of type j is given by

$$P_{ij}^{C} = \Delta t \, n_j u_0 2\pi \int_0^{\pi} \sigma_{ij}(u_0, \chi') \sin\chi' \, d\chi' \qquad (2)$$

where Δt is the time step, n_j is the density of the collision partner, u_0 is the electron speed prior to the collision (the neutral species are assumed to be motionally frozen relative to the electrons) and σ_{ij} is the differential cross section for the collision process of type i with a particle of type j. The latter is a function of the electron speed prior to collision and the scattering angle χ. A random number, r, uniformly distributed over [0,1] dictates whether the electron continues its trajectory unimpeded

$$r \leqslant P^{NC} \qquad (3)$$

or undergoes a collision of a specific type i (ionization, excitation, elastic and so on) with particle j (atomic and molecular species)

$$P^{NC} + \sum_{l=1}^{k-1} P_l^{C} \leqslant r < P^{NC} + \sum_{l=1}^{k} P_l^{C} \qquad (4)$$

where each value of l corresponds to a unique pair (i, j). Once the collision type has been determined, the energy of the electron is revised according to the collision characteristics (such as whether it is elastic or inelastic). The velocity of the electron is then updated based on the scattering and azimuthal angles. The scattering angle distribution function used in this study was uniform (that is, for isotropic scattering).

To account for production and loss of electrons (for example, by ionization and attachment), electrons are removed or added to maintain the number of simulated electrons within a specified range. Typically 100–300 electrons are initially assigned velocities randomly selected from a Maxwell–Boltzmann distribution with an average energy of 1 eV. On the first application of the DMC module, no statistics are recorded for the first 10–50 RF cycles so as to allow the electrons to relax to the applied electric field. On subsequent application of the DMC module, with updated electric field and gas composition, the electrons retain their velocity components as predicted by the previous application. Statistics are accumulated over 50–100 RF cycles.

As electrons are moved forward in time, the velocity components are recorded at specific times in the RF cycle (phase angles ϕ), and statistics are accumulated. Numerically, the time-dependent electron-energy distribution function (EEDF), $f(\varepsilon; \phi)$, is computed on discrete elements $\Delta\varepsilon_i \Delta\phi_j$ located around ε_i and ϕ_j. As the simulation advances in time, the appropriate (ε_i, ϕ_j) bins of the EEDF are updated. The time-dependent electron-impact rate coefficients, $k_{ij}(\phi)$, are obtained by numerically computing the integral

$$k_{ij}(\phi) = \left(\frac{2}{m}\right)^{1/2} \int_0^{\infty} \sigma_{ij}(\varepsilon) f(\varepsilon; \phi) \sqrt{\varepsilon} \, d\varepsilon. \qquad (5)$$

By computing the rate coefficients through direct integration over the EEDF, there is no need to resolve the EEDF, thereby reducing the computational burden. The DMC module provided all electron-impact rate coefficients as a function of phase in the RF cycle, which were needed in the rest of the modules. The collisional processes included in the simulation are shown in table 1. The cross sections for electron impact reactions have been given elsewhere [9, 10].

The DMC simulation method has some advantages over the null-collision Monte Carlo (NCMC) method, which is widely used to calculate the EVDF. The latter method requires the electron free-flight distribution (FFD) as an input to the simulation. In contrast, the DMC simulation does not require knowledge of the FFD. In fact, the free-flight distribution is an output of the DMC simulation. In addition, the DMC simulation requires fewer random numbers per time step to describe the stochastic electron collision processes, and no artificial processes (null collisions) are introduced.

2.1.2. Module II: neutral and ionic species density balances. Differential mass conservation equations were written for the heavy species (atomic and molecular neutral species and ions) for a spatially uniform plasma. In the case of a chlorine plasma, these balances become (see the nomenclature for meanings of symbols)

$$\frac{dn_{Cl}}{dt} = k_{att} n_e n_{Cl_2} + 2k_d n_e n_{Cl_2} + 2k_{ii} n_{Cl^-} n_{Cl^+} + k_{ii} n_{Cl^-} n_{Cl_2^+}$$
$$+ 2k_{ei} n_e n_{Cl_2^+} + u_{B1} n_{Cl^+} \frac{S_L h_{L,Cl^+} + S_R h_{R,Cl^+}}{V_{pl}}$$
$$- k_{i1} n_e n_{Cl} - 2k_{vr} n_{Cl}^2 N - \frac{n_{Cl}}{\tau_{res}} - \sum_j k_{sr,j} \frac{S_j}{V_{pl}} n_{Cl} \qquad (6)$$

Table 1. Important collision processes in a chlorine discharge.

Process	Reaction	Threshold energy (eV)
Electron impact reactions		
Dissociative excitation	$Cl_2 + e \rightarrow Cl_2^* (C\ ^1\Pi) + e \rightarrow 2Cl + e$	3.12
Electronic excitations (molecular)	$Cl_2 + e \rightarrow Cl_2^* + e$	
$B\ ^3\Pi$		2.49
$2\ ^1\Pi$ and $2\ ^1\Sigma$		9.25
Electronic excitations (atomic)	$Cl + e \rightarrow Cl^* + e$	
4s		8.90
4p		10.40
3d		10.90
5p		11.80
4d		12.00
5d		12.40
Vibrational excitation	$Cl_2 + e \rightarrow Cl_2^* + e$	0.0689
Molecular ionization	$Cl_2 + e \rightarrow Cl_2^+ + 2e$	11.47
Atomic ionization	$Cl + e \rightarrow Cl^+ + 2e$	12.99
Dissociative attachment	$Cl_2 + e \rightarrow Cl_2^{-*} \rightarrow Cl^- + Cl$	0.0
Electron–ion neutralization	$e + Cl_2^+ \rightarrow 2Cl$	0.0
Momentum transfer (atomic)	$e + Cl \rightarrow e + Cl$	0.0
Momentum transfer (molecular)	$e + Cl_2 \rightarrow e + Cl_2$	0.0
Other reactions		
Ion–ion recombination	$Cl_2^+ + Cl^- \rightarrow Cl_2 + Cl$	
Ion–ion recombination	$Cl^+ + Cl^- \rightarrow 2Cl$	
Volume recombination	$Cl + Cl + M \rightarrow Cl_2 + M$	

$$\frac{dn_{Cl^-}}{dt} = k_{att} n_e n_{Cl_2} - k_{ii} n_{Cl^-} n_{Cl^+} - k_{ii} n_{Cl^-} n_{Cl_2^+} - \frac{n_{Cl^-}}{\tau_{res}} \quad (7)$$

$$\frac{dn_{Cl^+}}{dt} = k_{i1} n_e n_{Cl^-} k_{ii} n_{Cl} n_{Cl^+} - u_{B1} n_{Cl^+} \frac{S_L h_{L,Cl^+} + S_R h_{R,Cl^+}}{V_{pl}} - \frac{n_{Cl^+}}{\tau_{res}}. \quad (8)$$

In order of appearance of the terms on the right-hand side of equation (6), atomic chlorine is produced by attachment to and dissociation of molecular chlorine, by ion–ion (volume) recombination, by dissociative electron–ion (volume) recombination of Cl_2^+ and by Cl^+ ion recombination on the reactor walls. It is lost by ionization, volume recombination, gas flow out of the reactor and wall recombination. In equation (7), negative Cl^- ions are produced by electron attachment and are lost by ion–ion recombination and gas flow. Negative ion losses to the walls of the reactor were assumed negligible because of the unfavourable potential gradient at the wall, which repels negative ions. In equation (8), positive Cl^+ ions are produced by ionization, and are lost by ion–ion recombination, flow to the walls and gas flow out of the reactor. In general, losses of charged particles by gas flow are negligible. However, gas flow may be an important loss mechanism for neutral particles. Wall recombination was taken to be linear in Cl density (assuming a surface saturated with Cl), thus

$$r_{sr} = k_{sr} n_{Cl} \quad (9)$$

with

$$k_{sr} = \frac{\gamma}{4} v_{th} = \frac{\gamma}{4} \left(\frac{8kT_g}{\pi M_{Cl}} \right)^{1/2} \quad (10)$$

where γ is a reaction probability particular to the surface of interest. In our case, we used $\gamma = 8.2 \times 10^{-3}$ for the substrate and for all other walls exposed to the plasma, except where noted. Also, h_{Ri} is a correction factor to account for the density drop of positive ion i from the bulk plasma to the radial sheath edge, h_{Li} is the corresponding correction factor for the axial sheath, and u_{Bi} is the Bohm velocity for that ion. An expression suggested by Godyak [7, 1] was used for the density correction factor written as

$$h_{Rj} = \frac{0.8}{(4 + R/\lambda_j)^{1/2}} \quad (11)$$

$$h_{Lj} = \frac{0.86}{\left[3 + \frac{L}{(2\lambda_j)}\right]^{1/2}} \quad (12)$$

where R and L are the dimensions of the source (figure 1) and λ_j is the mean free path of ion j. Equations (11) and (12) are applicable to electropositive discharges. They are expected also to be applicable to the HDP chlorine system under conditions of high power, low pressure and low values of the wall recombination probability γ of Cl atoms. Under these conditions the gas is highly dissociated (see results below) and the discharge is only slightly electronegative. When the

negative ion density becomes appreciable, correction factors can be introduced into equations (11) and (12). In view of the favourable agreement of our model predictions with available experimental data (see figures 6 and 8 later), we felt that such corrections were not necessary at this stage of development of the model.

The atomic and molecular species are too massive to respond to the rapid variations of the applied field. In addition, neutral and ionic species reactions occur over time scales much longer than the applied frequency. Thus the time derivatives of the heavy-species density were set equal to zero, neglecting the small variation over an RF period. The Cl_2^+ ion density was found by using the electroneutrality constraint

$$n_{Cl_2^+} = n_{Cl^-} + \langle n_e \rangle - n_{Cl^+} \tag{13}$$

where $\langle n_e \rangle$ is the time-average electron density. The Cl_2 density was obtained from an overall chlorine mass balance (the total number density was assumed constant).

2.1.3. Module III: electron density and power balance. This module consists of two nonlinear equations to determine the self-sustaining electric field (which is assumed to be sinusoidal) and the electron density waveform. The time-dependent electron density balance reads

$$\frac{dn_e}{dt} = k_{i1} n_{Cl} n_e + k_{i2} n_{Cl_2} n_e - k_{att} n_{Cl_2} n_e - \frac{n_e}{\tau_{res}} - \sum_j u_{Bj} n_j \frac{S_L h_{Lj} + S_R h_{Rj}}{V_{pl}} - k_{ei} n_{Cl_2^+} n_e. \tag{14}$$

Equation (14) is subject to the periodic steady state condition

$$\int_0^\tau \frac{dn_e}{dt}\, dt = 0. \tag{15}$$

The terms on the right-hand side of equation (14) account for electron production by ionization of atomic and molecular chlorine and for electron loss by attachment, gas flow, recombination on the walls of the container and electron–ion (volume) recombination. In the self-sustained discharge, the total charge flow to the walls must be balanced. Since negative ions are excluded from the walls, the electron current to the wall must equal the positive ion current over an RF cycle. This is the reason that the electron flux to the walls has been replaced by the ion flux as given by the summation term in equation (14), assuming singly charged ions. Again, gas flow is a negligible contributor to electron loss. Equation (14) may be integrated to yield an expression of the form

$$n_e(t) = n_e(0) f_h(k_j(t), n_j) + f_i(k_j(t), n_j). \tag{16}$$

Functions f_h and f_i depend on the density n_j of heavy species (obtained from module II), and the rate coefficients k_j, which, for electron-impact reactions, are taken from module I.

The power balance formulation is an extension of our previous work on higher pressure plasmas [10]. The main difference with the earlier work is that, in the low-pressure HDP examined here, significant power loss may occur because of ion acceleration and loss to the walls of the container. The power input to the system by the RF coil is consumed by the following processes: (i) electron power losses due to elastic and inelastic (excitations, ionizations, attachment and electron–ion volume recombination) collisions with neutral species and ions, (ii) power loss due to electron flow to the walls and (iii) power loss due to the positive ion flow to the walls. Neglecting two- step ionization, the power loss to electrons (mechanisms (i) and (ii)) is given by [10]

$$\frac{P_{el}}{V_{pl}} = \sum_{j,el} \frac{2m}{M_j} k_{mj} n_j n_e \langle \varepsilon \rangle + \sum_{j,inel} k_j n_j n_e \varepsilon_j + \sum_{j,ions} k_{ij} n_j n_e \langle \varepsilon \rangle \tag{17}$$

where k_{ij} is the ionization rate coefficient for process j and ε_j is the threshold energy for process j. In equation (17), the sums represent power loss due to elastic collisions, inelastic collisions and wall and volume recombination of electrons. The power consumed for ion acceleration towards the walls is

$$P_{ions} = \sum_j I_{sj} (V_p - V_f) S_j \tag{18}$$

where I_{sj} is given by equation (20) below. The total power supplied by the RF coil is

$$P_{total} = P_{el} + P_{ions}. \tag{19}$$

Note that additional power may be injected into the reactor by an RF supply biasing the substrate electrode (see below).

2.2. The sheath (module IV)

This module solves for the energy and flux of positive ions striking the wall, assuming a collisionless sheath (see assumption (ii) above). Although the EVDF may not be Maxwellian, electron fluxes through the sheath are calculated as if the distribution were Maxwellian at an equivalent electron 'temperature'. The latter is found from $kT_e = \frac{2}{3}\langle \varepsilon \rangle$, with the average electron energy $\langle \varepsilon \rangle$ computed through the EVDF. It was further assumed that the negative ion flux striking the walls is zero.

In HDP sources, plasma generation is substantially decoupled from the substrate bias and the plasma potential does not oscillate violently as in capacitively coupled systems (unless significant capacitive coupling from the coils exists). In general, ions respond not to this oscillating potential but rather to the time-average plasma potential V_p. Consider a substrate in contact with the plasma. An ion sheath separates the substrate from the bulk plasma. Positive ions are accelerated in the pre-sheath region and enter at the sheath edge with a velocity equal to the Bohm velocity. If the ion density at the sheath edge is n_{sj}, then the current density due

to ion j entering the sheath is (assuming singly charged ions)

$$I_{sj} = eu_{Bj}n_{sj} = e\left(\frac{kT_e}{M_j}\right)^{1/2} n_{sj} = e\left(\frac{kT_e}{M_j}\right)^{1/2} n_j h_{lj} \tag{20}$$

where h_{lj} is given by equations (11) and (12) and $l = R$ or L. Since the ion motion is 'down the potential hill' as long as $V_p > V_w$, the ion flux should not be affected by the potential difference between the plasma and the substrate. The electron current density through the sheath is given by [11]

$$I_e = en_e\frac{1}{4}\left(\frac{8kT_e}{\pi m}\right)^{1/2} \exp\left(\frac{e(V_w - V_p)}{kT_e}\right). \tag{21}$$

2.2.1. The case of a floating substrate. The potential of a floating substrate with respect to the plasma $V_f - V_p$ is given by the requirement that the electron and positive ion currents to the wall must be equal, that is

$$I_e = \sum_j I_{sj}. \tag{22}$$

Using equations (20)–(22), with I_e evaluated at $V_w = V_f$, one can obtain the floating potential $(V_f - V_p)$ for given bulk charge density and electron 'temperature'. The energy of ions striking the wall is equal to

$$\varepsilon_+ = e(V_p - V_f). \tag{23}$$

2.2.2. The case of a biased substrate. Assume that an RF bias with frequency $\omega = 2\pi f$ is applied to the substrate such that the substrate potential is given by

$$V_w = V_{DC} + V_{RF}\sin(\omega t) \tag{24}$$

where V_{DC} and V_{RF} are the DC and RF components of the substrate potential, respectively. Although the instantaneous electron and ion fluxes to the substrate may not balance, the total particle current flowing to the substrate must be zero over an RF cycle, since the substrate is capacitively coupled; hence

$$\sum_j \int_0^{2\pi/\omega} I_{sj}\,dt = \int_0^{2\pi/\omega} I_e(t)\,dt. \tag{25}$$

Now $I_e(t)$ is a function of time by virtue of the fact that $V_w = V_w(t)$. Assuming I_{sj} independent of time, the integral on the left-hand side of equation (25) can be evaluated immediately. The integral on the right-hand side of equation (25) can be shown to be

$$\int_0^{2\pi/\omega} I_e(t)\,dt = en_e\frac{1}{4}\left(\frac{8kT_e}{\pi m}\right)^{1/2}\frac{2\pi}{\omega} \times \exp\left(\frac{e(V_{DC} - V_p)}{kT_e}\right) J_0\left(i\frac{eV_{RF}}{kT_e}\right) \tag{26}$$

where $J_0(x)$ is the Bessel function of the first kind of zeroth order and $i = \sqrt{-1}$. By using equations (20), (25) and (26), $(V_{DC} - V_p)$ can be evaluated for given bulk charge densities, electron 'temperature' and V_{RF}. At high enough frequencies, the ions do not respond to the instantaneous sheath voltage but rather to the time-average sheath voltage. Thus, the ions strike the wall with energy

$$\varepsilon_+ = e(V_p - V_{DC}). \tag{27}$$

To be more precise, one should compare the applied frequency with the ion transit frequency. In HDP sources, sheaths are thin and ions may be able to traverse the sheath in times less than half the period of the commonly applied 13.56 MHz bias voltage. A spread in the ion energy distribution would then result. This has been studied extensively in connection with capacitively coupled systems [12].

3. Method of solution

The method of solution followed the modular approach shown in figure 2. An initial guess for the species densities and the electric field was used in module I to calculate the electron-impact reaction rate coefficients. These coefficients, together with the guessed initial values for the species densities, were used to integrate the balance equations (6)–(8) of module II. Using the output from module II, a corrected electron density and electric field were obtained from the electron density and power balances of module III. Module III was solved by applying a secant or bisection algorithm to find E/N, which is implicit in these equations (the electron density balance can only be satisfied at the self-sustained E/N). The ion flux and energy at the wall needed in modules II and III were obtained from the sheath module IV. Cycling between the modules was repeated until convergence to the periodic steady-state was attained. The execution time on a Hewlett Packard Apollo 735 workstation was approximately 30 min, or less than 1 min if the rate coefficients were predetermined and used in tabular form.

4. Results and discussion

The model input consists of a reaction mechanism, reaction cross sections, RF coil power, any bias power, total number density, frequency, reactor geometry and dimensions, wall recombination probabilities, substrate voltage (if any) and feed gas composition and flow rate. The model output consists of the neutral and charged species densities, the self-sustaining electric field, the corresponding EEDF and the positive ion flux and energy at the walls. The parameter values that are held fixed are shown in table 2. The reactor dimensions are those of the TCP tool used by Ra and Chen [13]. For the parameters that were varied, the base values and range examined are shown in table 3. A parametric investigation of the effects of power and pressure is discussed below.

Table 2. Parameters that were held constant.

Term	Symbol	Value
Cl volume recombination ($cm^6\ s^{-1}$)	k_{vr}	1.14×10^{-32}
Ion–ion recombination ($cm^3\ s^{-1}$)	k_{ii}	5.0×10^{-8}
Radius (cm)	R	15
Length (cm)	L	6
Gas temperature (K)	T_{gas}	500
Substrate area (cm^2)	A_w	315
Remaining wall area (cm^2)	A_0	1664

Table 3. Base parameter values and the ranges examined.

Term	Symbol	Base value	Range examined
Power (W)	P	300	300–1000
Flow rate (sccm)	Q_0	200	
Neutral species density (cm^{-3})	N	1.93×10^{14}	9.65×10^{13}–7.72×10^{14}
Gas pressure (mTorr)	P	10	5–50
Ion–neutral collision cross section (cm^2)	σ	1.20×10^{-14}	4.0×10^{-15}–3.90×10^{-14}
Cl wall reaction probability	γ	0.0082	0.10

Although a time-dependent periodic steady state was obtained as part of the solution, the time-average values are shown for most quantities, since these can be directly compared with experimental data. In the results shown below, the base case values were used (table 3) unless noted otherwise. All results were obtained without substrate bias.

Figure 3 shows the time-dependent atomic chlorine ionization coefficient $k_{i,Cl}$ together with the mean electron energy $\langle\varepsilon\rangle$ for a sinusoidal electric field with amplitude 1000 Td (RMS value 707 Td), which is in the range of values obtained for the self-sustaining field (see below). This result was obtained for a 95% Cl and 5% Cl_2 mixture. At a pressure of 10 mTorr (figure 3(*a*)), the EVDF is out of phase with respect to the electric field. This is reflected in the phase shift between $k_{i,Cl}$ (also $\langle\varepsilon\rangle$) and the field. At a pressure of 100 mTorr (figure 3(*b*)), the EVDF is nearly in phase with the field. Also, the field can couple energy to the electrons more efficiently because of there being more randomizing collisions at 100 mTorr (Joule heating). This is reflected in the higher electron energy, as compared with that at 10 mTorr, for the same field strength. Another characteristic drawn from figure 3 is the degree of modulation of the electron swarm parameters. At low pressures, the modulation is much less, because the EVDF does not have a chance to 'follow the field'.

4.1. The effect of power

The mole fraction of atomic Cl depends on the wall recombination probability γ. For low γ (the base case value was set to $\gamma = 0.0082$ [10], which corresponds to a first-order rate coefficient of $k_{sr} = 110$ cm s^{-1}, see equation (10)), the amount of Cl is very high even at low power densities. For instance, at 300 W power (0.071 W cm^{-3}), the Cl mole fraction exceeds 0.8. At low pressure, volume recombination of atomic chlorine is negligible. Under the conditions studied, the flow loss time constant is also long. Since wall recombination is also weak in this case, atomic chlorine builds up to a high steady-state value. For higher values of γ ($\gamma = 0.1$ or $k_{sr} = 1340$ cm s^{-1}, see the broken line in figure 4), wall recombination causes the Cl mole fraction to drop considerably. Of course, in the presence of etchable material (such as silicon or aluminium) the chlorine density will be even lower. Figure 4 also shows the effect of using a different cross section for the ion–molecule (atom) collisions.

A comparison of the charged species' densities is made in figure 5. The dominant ion is Cl^+, which is consistent with the very high degrees of dissociation achieved in the system. The density of the molecular Cl_2^+ ion is 2–15 times lower. The negative ion density is lower than the electron density above power levels of about 300 W. This is in contrast to higher pressure (> 100 mTorr) Cl_2 discharges, for which the negative (and positive) ion density is orders of magnitude higher than the electron density [9, 10]. High-pressure discharges in Cl_2 are strongly electronegative, whereas, at low pressure and high power density, the chlorine discharge becomes only moderately electronegative. The negative ion density decreases with increasing power as the gas becomes dissociated further. At the same time, the electron density increases, making the discharge less and less electronegative as the power is increased. The plasma density increases almost linearly with increasing power. Similar findings were reported by Lee *et al* [6] for an oxygen discharge.

Figure 6 shows the total (atomic plus molecular) ion flux bombarding the substrate electrode as a function of power. As the ion–molecule collision cross section is increased, the total flux decreases. The wall recombination coefficient of atomic chlorine does not

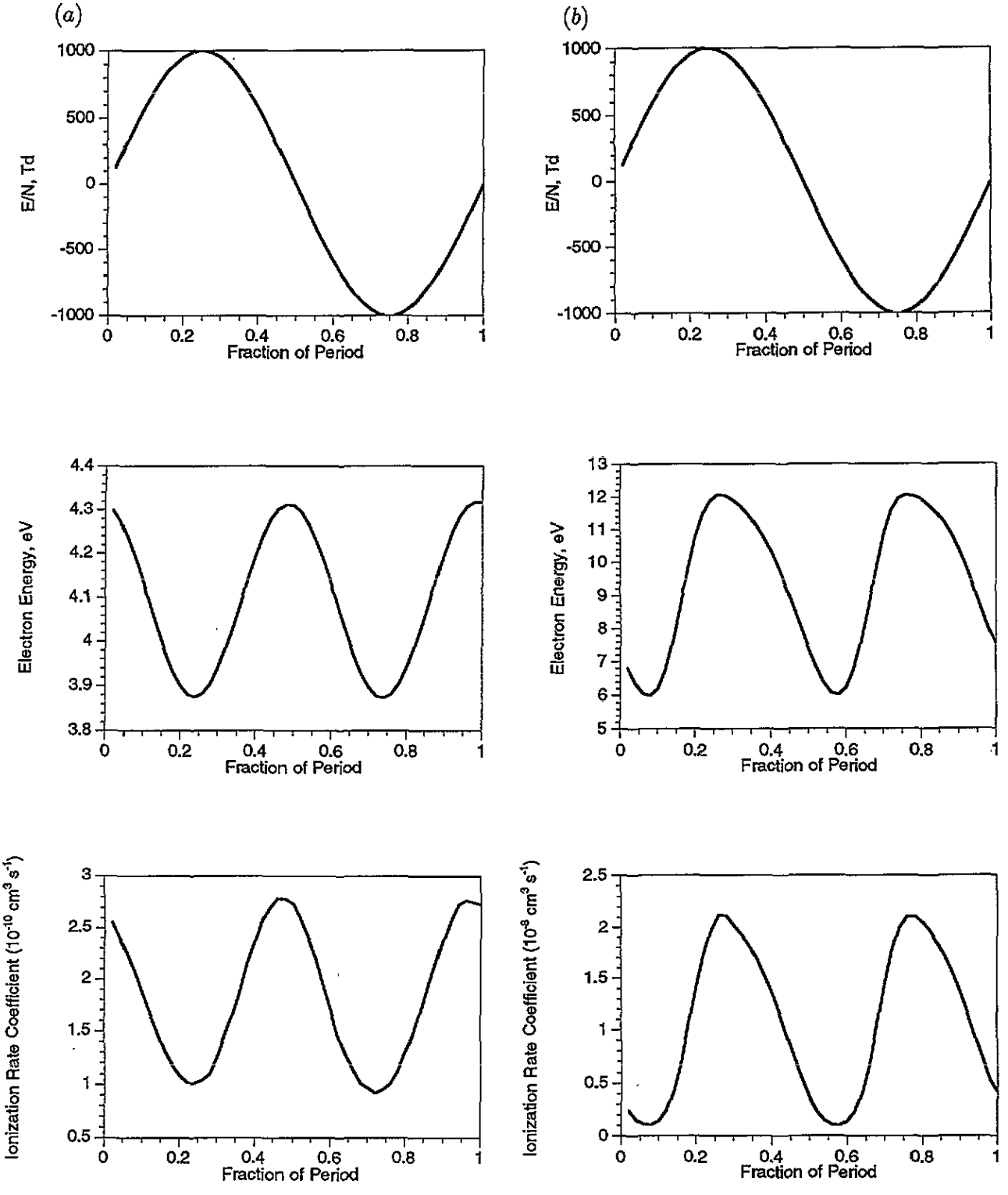

Figure 3. The applied electric field to neutral density ratio E/N (Td, top), mean electron energy (eV, middle), and atomic chlorine ionization rate coefficient (cm^3 s^{-1}, bottom), for (*a*) 10 mTorr and (*b*) 100 mTorr. The gas composition was 95% Cl and 5% Cl_2.

seem to have an appreciable effect on the total ion flux. However, the individual ion fluxes (not shown) are indeed affected. Ra and Chen [13] reported relative values of ion current density as a function of power in a Lam TCP-9600 reactor. The data are within a factor of two of the predicted values. This agreement is considered satisfactory, given the fact that no rate coefficients were adjusted (the wall recombination coefficient γ is the only unknown, but the total ion flux is insensitive to γ), and the ion flux measurements (by Langmuir probes) are probably correct to within a factor of two.

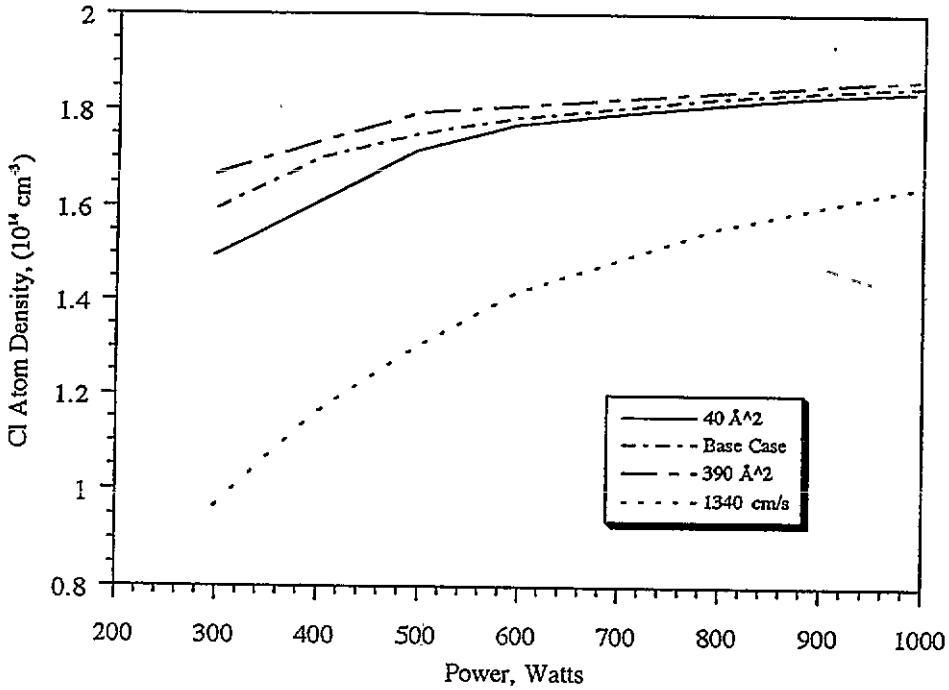

Figure 4. The atomic chlorine density as a function of power for various ion–neutral collision cross sections. A case with wall recombination rate coefficient of 1340 cm s^{-1} is also shown. Other parameters are at their base values (table 3).

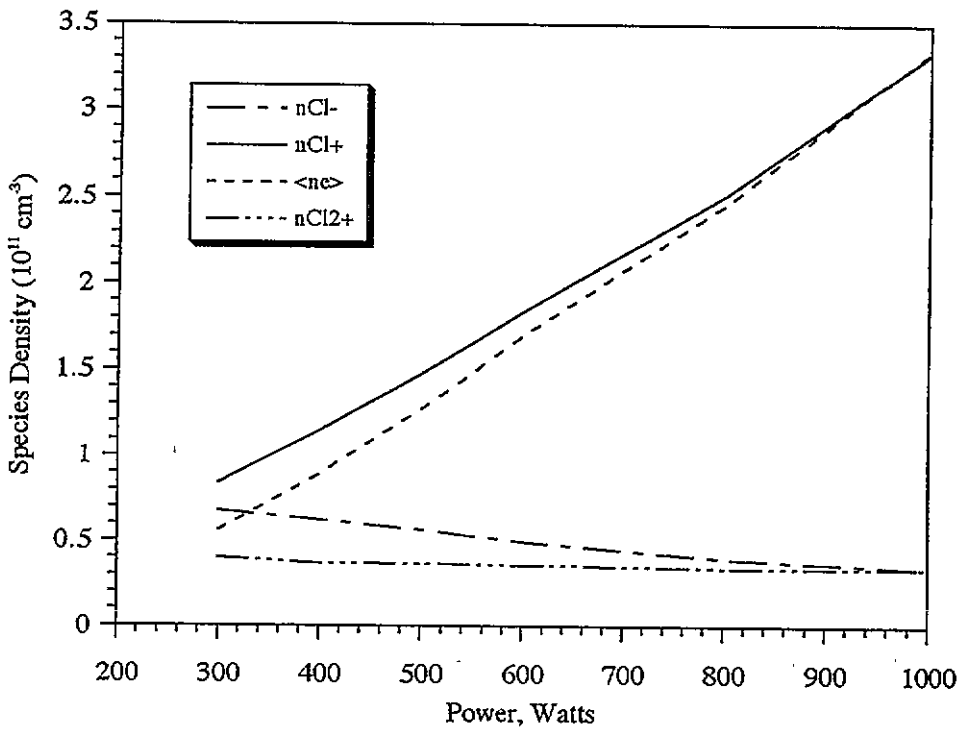

Figure 5. Electron, positive and negative ion densities as a function of power. Other parameters are at their base values (table 3).

Over the range of power studied (300–1000 W), the self-sustaining electric field to neutral density ratio E/N decreased from 690 to 670 Td (RMS value). The weak dependence of the sustaining field on power is understood for a system based on a single-step ionization mechanism.

4.2. The effect of pressure

The electron and ion densities as a function of pressure are shown in figure 7. The electron density decreases significantly with pressure, in part because the electron energy drops with increasing pressure, causing a drop in the ionization rate. Also, attachment to molecular

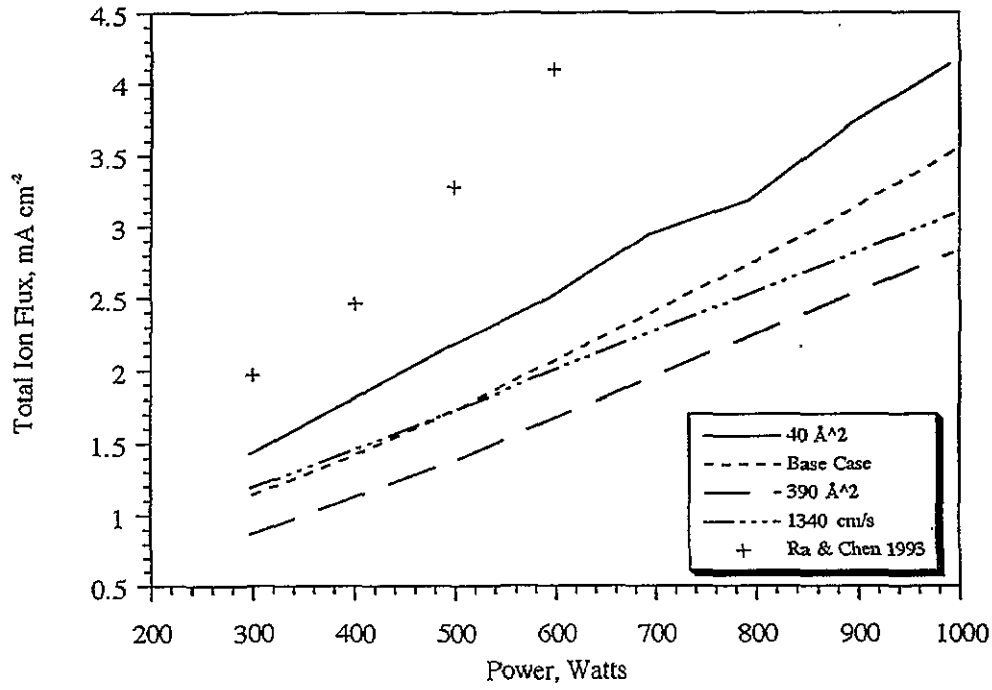

Figure 6. The ion current density as a function of power for various ion–neutral collision cross sections. Other parameters are at their base values (table 3). Data of Ra and Chen [13] are shown by crosses.

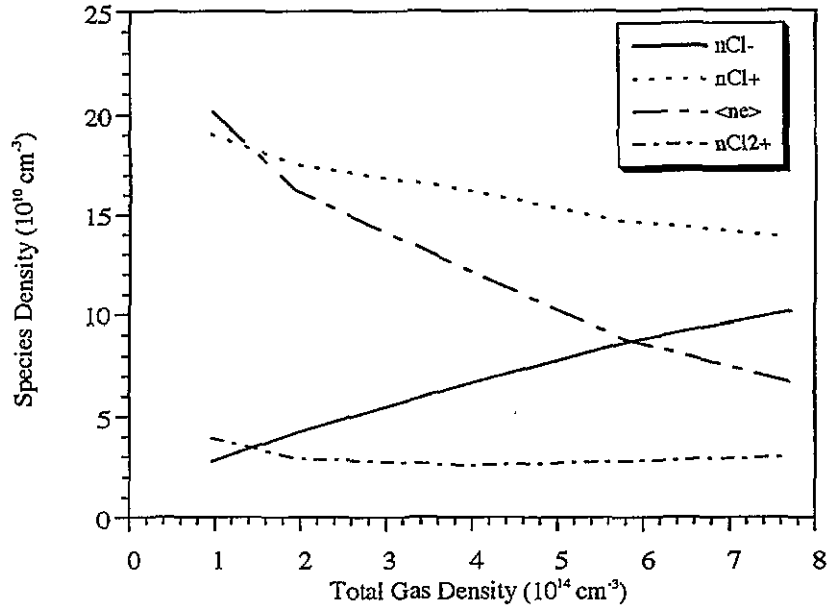

Figure 7. Electron, positive and negative ion densities as a function of total gas number density. Other parameters are at their base values (table 3).

chlorine becomes progressively more important as pressure increases. The negative ion density increases with pressure and exceeds the electron density beyond 6×10^{14} cm^{-3}, under the conditions examined. Thus the degree of electronegativity of the discharge increases with pressure. The ion density (especially the total ion density) is rather insensitive to pressure, although the ion flux does decrease with pressure (figure 8). The data of Ra and Chen [13] are again in satisfactory agreement with the calculation. A similar trend was observed by Patrick *et al* [14].

The self-sustaining E/N (RMS value) is shown in figure 9 as a function of pressure. A dramatic drop in E/N is observed as pressure increases. At low pressures, it is very difficult to couple energy into the electron gas through collisional heating just because

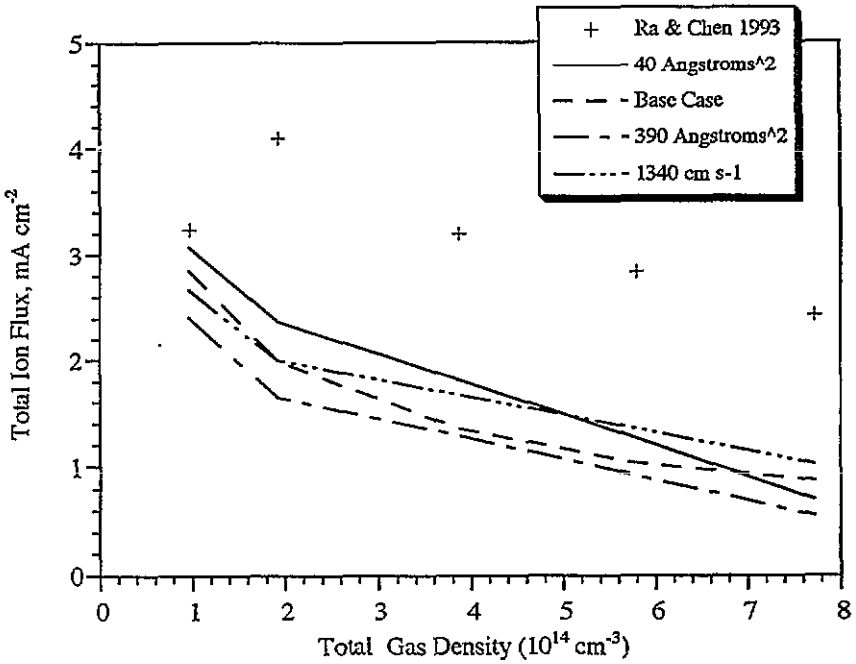

Figure 8. The ion flux as a function of total gas density for various ion–neutral collision cross sections and for a power of 600 W. Other parameters are at their base values (table 3). Data of Ra and Chen [13] are shown by crosses.

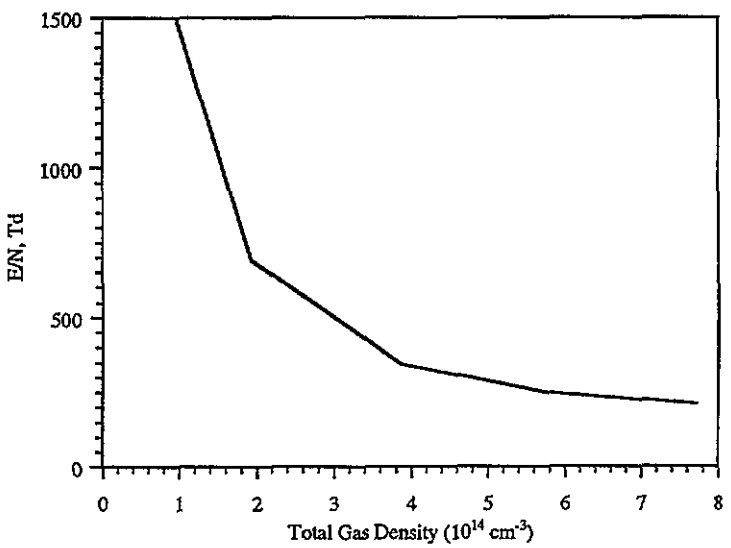

Figure 9. The self-sustaining electric field (RMS value) as a function of total gas density. Other parameters are at their base values (table 3).

there are very few collisions of the electrons with the background gas. This is manifested in the large phase shift between the applied field and the electron energy (see figure 3(*a*)). The discharge acts as an inductor. A very large electric field is then required to impart enough energy to the electrons to produce ionization to sustain the discharge. As the pressure increases, more collisions between electrons and the gas facilitate energy transfer to the electrons, making the discharge less inductive and more resistive. The phase shift between the field and the electron energy becomes smaller (see figure 3(*b*)). A smaller E/N is then necessary in order to sustain the discharge. In addition, as pressure increases, the charge flow to the walls decreases. Thus, the ionization rate required to sustain the discharge decreases. The self-sustaining E/N decreases correspondingly.

Collisionless heating in a spatially varying electric field may become important at low pressures [15, 16]. Of course, this heating mechanism cannot be captured by the spatially average model of the bulk plasma. The result of collisionless heating can be thought of as an increase in the *effective* electron–neutral species

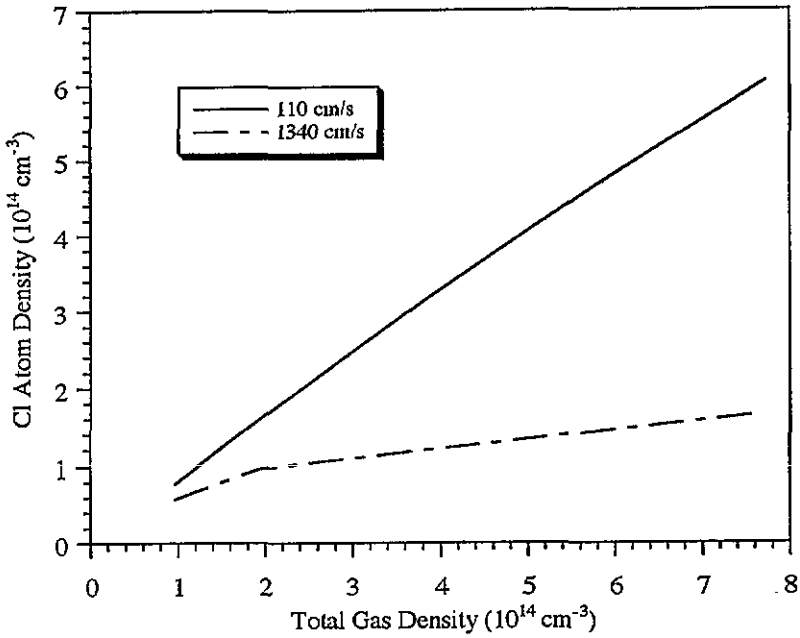

Figure 10. The atomic chlorine density as a function of total gas density for two values of the wall recombination rate coefficient. Other parameters are at their base values (table 3).

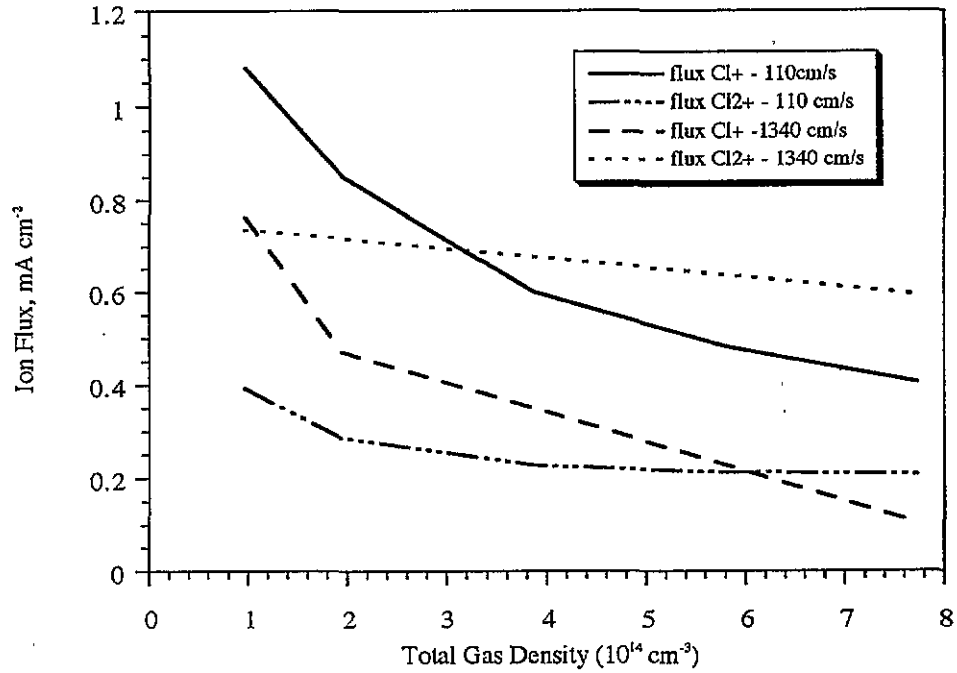

Figure 11. The ion flux as a function of total gas density for two values of the wall recombination rate coefficient. Other parameters are at their base values (table 3).

collision frequency [16]. Thus, at low pressures, the actual electric field required to sustain the discharge will be lower than that predicted by figure 9.

4.3. The effect of wall recombination

The effect of the wall recombination probability on the Cl atom density as a function of power is shown in figure 4. Figure 10 shows that the Cl atom density increases with total gas density. This is because of the availability of more molecules to be dissociated. For low values of the wall recombination probability γ, the gas is greatly dissociated into atoms. However, the Cl atom mole fraction can be less than 0.2 for high values of γ. Under these conditions the dominant neutral species is Cl_2 and the negative ion density far exceeds the electron density. Figure 11 shows the atomic and molecular ion flux also as a function of total gas density. The molecular

ion flux dominates at higher pressures and higher wall recombination probabilities.

4.4. The effect of metastable atoms

Metastable chlorine atoms, Cl^*, need to be examined since Cl may be the dominant neutral species under conditions of high power and low pressure. The importance of Cl^* was examined by the addition of a species density balance for a lumped metastable state to the rest of the equations. Metastable atoms were produced by excitation from ground state Cl atoms; they were lost by ionization and diffusion to the reactor walls. Appropriate modifications to the atomic chlorine balance (equation (6)), electron density balance (equation (14)) and power balance (equation (17)) were also made. The excitation and ionization cross sections were estimated based on the shape of the corresponding ground state cross sections, but shifted by the energy of the metastable levels. A limited number of runs showed that metastable species did not have a significant effect on the plasma gas composition. This may be due to the rather low energy content of the Cl metastable species combined with the high values of E/N found in HDP sources. Under these circumstances direct ionization from the ground state dominates over two-step ionization through the metastable level. A similar conclusion was reached by Lee *et al* [6] regarding the influence of metastable oxygen atoms in a HDP oxygen system. Metastable species have been found to have a dramatic effect in relatively high pressure (greater than a few hundred milli-Torr) argon discharges [17, 18].

5. Summary

A two-region model of a low-pressure, high-density plasma was developed using a modular approach. A spatially uniform (zero-dimensional) model of the bulk plasma was coupled to an analytic model for a collisionless sheath. The time-dependent electron velocity distribution function and associated rate coefficients were calculated by a dynamic Monte Carlo (DMC) algorithm. By decoupling the heavy (neutral species, ions) from the light (electrons) species equations, the vastly disparate time scales of the problem were handled in a computationally efficient manner. The model requires as input the reaction mechanism and pertinent reaction cross sections, the reactor geometry and operating conditions. The output of the model is the density of neutral and charged species, the EVDF and the flux and energy of positive ions bombarding the walls.

The model was applied to a chlorine discharge sustained in a HDP reactor. The results of the simulation can be summarized as follows.

(i) For small values of the wall recombination probability γ of Cl atoms, the molecular gas dissociation is very high. Correspondingly, the dominant positive ion is Cl^+. For high values of γ, the dominant positive ion is Cl_2^+.

(ii) The total (atomic plus molecular) ion flux bombarding the wall is insensitive to the value of γ, but is somewhat dependent on the cross section for ion–molecule (atom) collisions. The total ion flux increases with power, but decreases with pressure in the range studied.

(iii) The electron and positive ion densities increase almost linearly, but the negative ion density drops with power. As pressure increases, the electron density decreases, the negative ion density increases and the total positive ion density remains almost constant.

(iv) In contrast to high-pressure, low-density chlorine discharges, which are strongly electronegative, the low-pressure HDP is only moderately electronegative. The discharge becomes more electronegative on decreasing the power, increasing the pressure or increasing γ.

(v) The self-sustaining electric field is a weak function of power, but decreases strongly with increasing pressure.

(vi) Metastable chlorine atoms appear to have no significant effect on the plasma chemistry under low-pressure, high-density conditions.

Model predictions were compared with experimental data on ion flux as a function of pressure and power in a Lam TCP 9600 tool. The agreement was deemed satisfactory considering that no adjustments were made in any model parameters and that the experimental data are uncertain to within a factor of two. The only variable parameters in the model are the ion–neutral species collision cross section and γ. The former has a rather minor effect on the ion flux (varying the cross section by an order of magnitude changes the flux by only about 75%). The latter has an even smaller effect. It is interesting to note that the Bohm velocity used to calculate the ion flux (equation (20)) is applicable for an electropositive plasma. The chlorine plasma is moderately electronegative, yet the model provides reasonable quantitative predictions of the ion flux. However, detailed two-dimensional calculations of a chlorine HDP have shown that the negative ions accumulate near the maximum of the plasma potential, and their density is very low near the plasma–sheath interface. Under these conditions, the Bohm velocity based on an electropositive plasma may be a reasonable approximation.

Results presented in this paper have been for an 'empty' reactor without a silicon wafer present. Later studies will address the problem of polysilicon etching using a TCP reactor. Capacitive coupling can be included by adding the extra power given to the electrons by the oscillating sheath (most of the power is used to accelerate ions). Also, the model formulation is sufficiently general to incorporate more complex gas chemistries. In particular, mixed gas (such as $Ar–Cl_2$) discharges are of interest due to their importance in semiconductor fabrication. Finally, application of the model to ECR discharges is easier since the EEDF does not respond to the microwave field. For this case one does not need to solve for the time-dependent EVDF or any time-dependent balance equations.

Acknowledgments

Financial support for this project was provided by Sandia National Laboratories under a CRADA with Sematech, the National Science Foundation (CTS-9216023) and The Welch Foundation.

Note added in proof. Recently we became aware of the work of Meeks and Shon [19] which is similar to that described in this paper. These authors used a well-mixed (0-D) time-independent approximation to model plasma etch processes, including complex gas-phase and surface reactions. They examined the effect of the electron energy distribution function (EEDF) on the species densities in the plasma. They found that a Maxwellian EEDF can overestimate the electron density by less than a factor of two (as compared with the EEDF calculated by a Boltzmann solver).

References

[1] Lieberman M A and Gottscho R A 1993 Design of high density plasma sources for materials processing *Physics of Thin Films* ed M Francompe and J Vossen (Orlando, FL: Academic)
[2] Lymberopoulos D P and Economou D J 1994 *J. Vac. Sci. Technol.* A **12** 1229
[3] Ventzek P L G, Hoekstra R J and Kushner M J 1994 *J. Vac. Sci. Technol.* B **12** 461
[4] Economou D J and Alkire R C 1988 *J. Electrochem. Soc.* **135** 2786
[5] Aydil E S and Economou D J 1993 *J. Electrochem. Soc.* **140** 1471
[6] Lee C, Graves D B, Lieberman M A and Hess D W 1994 *J. Electrochem. Soc.* **141** 1546
[7] Godyak V A 1986 *Soviet Radio Frequency Discharge Research* (Falls Church, VA: Delphic Associates)
[8] Lymberopoulos D P and Economou D J 1995 *J. Phys. D: Appl. Phys.* to be published
[9] Aydil E S and Economou D J 1992 *J. Electrochem. Soc.* **139** 1396
[10] Deshmukh S C and Economou D J 1992 *J. Appl. Phys.* **72** 4597
[11] Chapman B 1980 *Glow Discharge Processes* (New York: Wiley)
[12] Metze A, Ernie D W and Oskam H J 1989 *J. Appl. Phys.* **65** 993
[13] Ra Y and Chen C H 1993 *J. Vac. Sci. Technol.* A **11** 2911
[14] Patrick R and Bose F *46th Gaseous Electronics Conf., Montréal, October 1993* paper LD-5
[15] Turner M M 1993 *Phys. Rev. Lett.* **71** 1844
[16] Godyak V A, Piejak R B and Alexandrovich B M *46th Gaseous Electronics Conf., Montréal, October 1993* paper NA-6
[17] Lymberopoulos D P and Economou D J 1993 *J. Appl. Phys.* **73** 3668
[18] Ferreira C M and Richard A 1983 *J. Appl. Phys.* **54** 2261
[19] Meeks E and Shon J W 1995 *IEEE Trans. Plasma Sci.* to be published